PAPER *Special Section on Advanced Technologies in Antennas and Propagation in Conjunction with Main Topics of ISAP2009*

Three-Dimensional Electromagnetic Scattering Analysis Using Constrained Interpolation Profile Method

Jerdvisanop CHAKAROTHAI[†a)], ***Student Member***, **Qiang CHEN**[†], ***Member***, ***and*** **Kunio SAWAYA**[†], ***Fellow***

SUMMARY A characteristic-based constrained interpolation profile (CIP) method for solving three-dimensional, time-dependent Maxwell's equations is successfully developed. It is utilized to solve one-dimensional wave equations in the formulation of the Maxwell's equations. Calculation procedure of the CIP method for three-dimensional scattering analysis is described in details. Update equations for boundary conditions of a perfectly conducting (PEC) interface and a dielectric interface are formulated and obtained in explicit forms. Numerical analyses of electromagnetic scatterings of PEC sphere, dielectric sphere and PEC cube are performed and the scattering coefficient is calculated and compared with the Mie's analytic results. As a result, the scattering coefficients show good agreement with the Mie's results, which demonstrates the validity of the CIP method and the formulated update equations. It is also shown that the phase of the scattering coefficients determined by the CIP method are slightly more accurate than that of the FDTD method.

key words: *electromagnetic scattering analysis, scattering cross section, CIP method, FDTD method, Mie*

1. Introduction

The field of computational electromagnetics (CEM) has been significantly broadened by the pioneer work of Yee, when the time-dependent Maxwell's equations are solved numerically in isotropic medium [1]. Yee's algorithm has been called the finite-difference time-domain (FDTD) method and it has a second-order accuracy in temporal and spatial domains [2]. Since the FDTD method is relatively simple to implement, efficient and robust, so it has been widely applied to many types of electromagnetic problems, and also implemented in many kinds of commercial softwares nowadays. When the FDTD method is used to analyze a problem using a time step size restricted by the Courant-Friedrichs-Lewy (CFL) stability condition, it was shown analytically that there is no dissipative error in the solution obtained by the FDTD method [2]. However, the FDTD method suffers from numerical dispersion or anisotropy, i.e. numerical propagation velocity of electromagnetic wave depends on cell size, time step size, and direction of propagation. This anisotropy causes an accumulative phase error and restricts the analysis solution to the Rayleigh or resonance region where electrical length is in the order of a few wavelengths.

In previous studies, a numerical method, which was developed from a characteristic-based scheme for solving Euler equations in the field of computational fluid dynamics (CFD), has been applied for solving the time-domain Maxwell's equations [3]–[7]. The coefficient matrices in the Maxwell's equations are diagonalized in each spatial direction to obtain one-dimensional Riemann formulation for both Cartesian coordinate system and general curvilinear system. Then, a windward difference formulation, i.e. forward or backward difference method, has been used to solve the one-dimensional Riemann problems derived from the eigenvalue analysis and it was shown that the numerical stability can be improved by using the characteristic-based method [6], [8]. In addition, analysis accuracy can be improved by using high-order interpolation or extrapolation technique.

Recently, an application of the characteristic-based constrained interpolation profile (CIP) method to the field of CEM was proposed by Yabe et al. and since then it has been continuously received an attention from researchers [9], [10]. The CIP method is a kind of high-order interpolation method which can accurately solve the hyperbolic equations with third-order accuracy in spatial domain and provides a solution with a small phase error [11].

The CIP method has several advantages over the FDTD method. First, the CIP method can suppress reflected waves from the truncated region by simply forbidding the incoming wave propagation from the far region, whereas the absorbing boundary condition is required in the FDTD method and it actually relates to the complicated formulation of the Maxwell's equations. This attribute of the CIP method is inherited from the characteristic formulation, which can eliminate the reflected waves completely, if one of the transformed coordinates is aligned with the direction of the electromagnetic waves. Second, the formulation for the CIP method gives a directional biased discretization in spatial domain, which exhibits the physics in directional propagation in accordance with the sign of the eigenvalues, and provides a more stable scheme than a central differencing scheme [4]. Third, phase characteristic of the CIP method shows a better performance than the FDTD method over a broad range of frequencies as shown in [12]. Last, the CIP method allows a waveform which changes abruptly with respect to time, e.g. a rectangular pulse. In spite of many advantages of the CIP method, it also encounters two difficulties. First, since the calculation using the CIP method is the two-step scheme, i.e. the interpolation and the field updating for the field variables and their differential field variables, in

Manuscript received January 4, 2010.
Manuscript revised May 7, 2010.
[†]The authors are with the Department of Electrical and Communication Engineering, Tohoku University, Sendai-shi, 980-8579 Japan.
a) E-mail: jerd@ecei.tohoku.ac.jp
DOI: 10.1587/transcom.E93.B.2619

each time step, the computation time of the CIP method is more expensive than the FDTD method, which directly update each field variable with an explicit equation. Moreover, the CIP method uses more memory than the FDTD method because the derivative values of the each field component must be also stored in the memory. Second, the CIP method exhibits a dissipation error after a long-time propagation which is one of the disadvantages of the characteristic-based method.

In [12], it has been shown that the CIP method provides higher accuracy than the FDTD method under the condition of identical cell size of analysis by calculating the electromagnetic field radiated from uniform line current source. However, a three-dimensional scattering analyses of perfectly electric conducting (PEC) and dielectric objects using the CIP method have not been reported so far.

This paper proposes an approach utilizing the CIP method to solve the three-dimensional EM scattering problem and shows algorithms that enable the PEC and the dielectric objects to be modeled into the analysis region. The scattering cross sections (SCS) of PEC sphere and dielectric sphere demonstrate the validity and the possibility of the CIP method as an alternative CEM tool.

The rest of the paper is organized as follows. Section 2 reviews the formulation of the Maxwell's equations in Cartesian coordinate system and shows the calculation procedure for the three-dimensional CIP method in details. Section 3 shows the treatment of boundary conditions for PEC and dielectric interfaces and also boundary conditions at truncated region in the CIP method. Finally, analysis models and numerical results of the SCSs of various objects are shown in Sect. 4, and followed by our conclusion in Sect. 5.

2. Formulation of Maxwell's Equations

The time-dependent Maxwell's equations [15] for electromagnetic fields in isotropic medium are expressed as

$$\frac{\partial(\varepsilon\mathbf{E})}{\partial t} = \nabla\times\mathbf{H} - \mathbf{J}, \tag{1}$$

$$\frac{\partial(\mu\mathbf{H})}{\partial t} = -\nabla\times\mathbf{E}, \tag{2}$$

where $\mathbf{E}$ and $\mathbf{H}$ are the electric and magnetic field strength vectors in volts per meter and amperes per meter, respectively, and $\mathbf{J}$ is the current density in amperes per square meter. ε and μ are the permittivity and the permeability of the medium, respectively.

The Maxwell's equations in free space can be expressed in the conservative form in Cartesian coordinate system as

$$\frac{\partial\mathbf{W}}{\partial t} + \frac{\partial\mathbf{F}_x}{\partial x} + \frac{\partial\mathbf{F}_y}{\partial y} + \frac{\partial\mathbf{F}_z}{\partial z} = 0, \tag{3}$$

where $\mathbf{F}_x$=$A\mathbf{W}$, $\mathbf{F}_y$=$B\mathbf{W}$, and $\mathbf{F}_z$=$C\mathbf{W}$, $\mathbf{W} = (E_x\ E_y\ E_z\ H_x\ H_y\ H_z)^T$, where superscript T denotes transpose matrix. The coefficient matrices A, B, and C are given by

$$A = \begin{pmatrix} 0 & 0 & 0 & 0 & 0 & 0 \\ 0 & 0 & 0 & 0 & 0 & \varepsilon^{-1} \\ 0 & 0 & 0 & 0 & -\varepsilon^{-1} & 0 \\ 0 & 0 & 0 & 0 & 0 & 0 \\ 0 & 0 & -\mu^{-1} & 0 & 0 & 0 \\ 0 & \mu^{-1} & 0 & 0 & 0 & 0 \end{pmatrix}, \tag{4}$$

$$B = \begin{pmatrix} 0 & 0 & 0 & 0 & 0 & -\varepsilon^{-1} \\ 0 & 0 & 0 & 0 & 0 & 0 \\ 0 & 0 & 0 & \varepsilon^{-1} & 0 & 0 \\ 0 & 0 & \mu^{-1} & 0 & 0 & 0 \\ 0 & 0 & 0 & 0 & 0 & 0 \\ -\mu^{-1} & 0 & 0 & 0 & 0 & 0 \end{pmatrix}, \tag{5}$$

$$C = \begin{pmatrix} 0 & 0 & 0 & 0 & \varepsilon^{-1} & 0 \\ 0 & 0 & 0 & -\varepsilon^{-1} & 0 & 0 \\ 0 & 0 & 0 & 0 & 0 & 0 \\ 0 & -\mu^{-1} & 0 & 0 & 0 & 0 \\ \mu^{-1} & 0 & 0 & 0 & 0 & 0 \\ 0 & 0 & 0 & 0 & 0 & 0 \end{pmatrix}. \tag{6}$$

Eigenvalues of coefficient matrices A, B and C are found to be zero and $\pm c$, where c denotes the velocity of the electromagnetic wave in medium. The eigenvalues have multiplicities and hence the corresponding eigenvectors are not unique. However, in Cartesian coordinate system, linearly independent equations of the system still have been found by the orthogonalization of the coefficient matrices. When the similar matrices of diagonalization are known, the coefficient matrices can be diagonalized individually, and by using a straight-forward matrix multiplication, the diagonalized matrices are expressed as

$$D_x = S_x^{-1}AS_x, \quad D_y = S_y^{-1}BS_y, \quad D_z = S_z^{-1}CS_z, \tag{7}$$

where diagonal elements of D_x, D_y and D_z are equal to the eigenvalues of A, B and C, respectively, i.e.

$$\mathrm{Diag}(D_m) = \{c, c, -c, -c, 0, 0\}, \quad m = x, y, z. \tag{8}$$

S_m in (7) denotes a non-singular similar matrix composed of eigenvectors as a column vector and S_m^{-1} is its inverse matrix. The similar matrices and its inverse matrices associated with the coefficient matrices A, B and C are given in [3] and they will be omitted here. Since each coefficient matrix can only be diagonalized in x, y, and z axes individually, the three-dimensional problem is split into three one-dimensional systems:

$$\frac{\partial\mathbf{W}}{\partial t} + \frac{\partial(A\mathbf{W})}{\partial x} = 0, \quad (\mathbf{W}^n \to \mathbf{W}^*), \tag{9}$$

$$\frac{\partial\mathbf{W}}{\partial t} + \frac{\partial(B\mathbf{W})}{\partial y} = 0, \quad (\mathbf{W}^* \to \mathbf{W}^{**}), \tag{10}$$

$$\frac{\partial\mathbf{W}}{\partial t} + \frac{\partial(C\mathbf{W})}{\partial z} = 0, \quad (\mathbf{W}^{**} \to \mathbf{W}^{n+1}), \tag{11}$$

where, $\mathbf{W}^n$ is the field at a time step index n and $\mathbf{W}^*$ represents the field after propagating along the x direction. $\mathbf{W}^{**}$

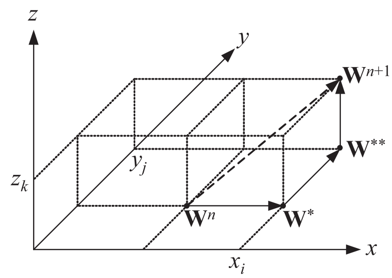

Fig. 1 Field translation in each propagation axis.

represents the field after propagating along the x and y directions. $\mathbf{W}^{n+1}$ represents the field after propagating along the x, y and z directions as shown in Fig. 1. Substituting (7) into (9), we obtain

$$\frac{\partial \mathbf{W}}{\partial t} + \frac{\partial (S_x D_x S_x^{-1} \mathbf{W})}{\partial x} = 0. \tag{12}$$

The similar matrix of the diagonalization and the eigenvalues are brought out of the differential operator to form one-dimensional hyperbolic equations which can be solved by the CIP method. First, we multiply the inverse of the similar matrix from the left side to give

$$\frac{\partial (S_x^{-1}\mathbf{W})}{\partial t} + D_x \frac{\partial (S_x^{-1}\mathbf{W})}{\partial x} = 0. \tag{13}$$

and for y and z direction, we obtain

$$\frac{\partial (S_y^{-1}\mathbf{W})}{\partial t} + D_y \frac{\partial (S_y^{-1}\mathbf{W})}{\partial y} = 0, \tag{14}$$

$$\frac{\partial (S_z^{-1}\mathbf{W})}{\partial t} + D_z \frac{\partial (S_z^{-1}\mathbf{W})}{\partial z} = 0. \tag{15}$$

The equations in (13), (14), and (15) are simply the one-dimensional wave equations and $S_x^{-1}\mathbf{W}$, $S_y^{-1}\mathbf{W}$ and $S_z^{-1}\mathbf{W}$ are the Riemann invariants or the characteristic variables which hold a constant value along a trajectory in both time and space, with a slope defined by corresponding eigenvalues. Since every equation is completely uncoupled each other, the system of equations can be solved individually as one-dimensional problem, and the CIP method is applied here to solve the equations of the system. The details of the CIP method are described in [10] and will be omitted here.

It should be noted that the calculation procedure is different from previous studies which use the finite-difference or the finite volumn method to solve the equations [4], [5]. The characteristic variables are advected forward or backward depending on the associated sign of its eigenvalues in the formulation. The equations for each characteristic variable in each propagation direction can be written as follows. For x direction,

$$L_{x+}^1 : \left(\frac{\partial}{\partial t} + c\frac{\partial}{\partial x}\right)\left(H_z + \frac{E_y}{\eta}\right) = 0, \tag{16}$$

$$L_{x-}^1 : \left(\frac{\partial}{\partial t} - c\frac{\partial}{\partial x}\right)\left(H_z - \frac{E_y}{\eta}\right) = 0, \tag{17}$$

$$L_{x+}^2 : \left(\frac{\partial}{\partial t} + c\frac{\partial}{\partial x}\right)\left(H_y - \frac{E_z}{\eta}\right) = 0, \tag{18}$$

$$L_{x-}^2 : \left(\frac{\partial}{\partial t} - c\frac{\partial}{\partial x}\right)\left(H_y + \frac{E_z}{\eta}\right) = 0, \tag{19}$$

for y direction,

$$L_{y+}^1 : \left(\frac{\partial}{\partial t} + c\frac{\partial}{\partial y}\right)\left(H_z - \frac{E_x}{\eta}\right) = 0, \tag{20}$$

$$L_{y-}^1 : \left(\frac{\partial}{\partial t} - c\frac{\partial}{\partial y}\right)\left(H_z + \frac{E_x}{\eta}\right) = 0, \tag{21}$$

$$L_{y+}^2 : \left(\frac{\partial}{\partial t} + c\frac{\partial}{\partial y}\right)\left(H_x + \frac{E_z}{\eta}\right) = 0, \tag{22}$$

$$L_{y-}^2 : \left(\frac{\partial}{\partial t} - c\frac{\partial}{\partial y}\right)\left(H_x - \frac{E_z}{\eta}\right) = 0, \tag{23}$$

and for z direction,

$$L_{z+}^1 : \left(\frac{\partial}{\partial t} + c\frac{\partial}{\partial z}\right)\left(H_y + \frac{E_x}{\eta}\right) = 0, \tag{24}$$

$$L_{z-}^1 : \left(\frac{\partial}{\partial t} - c\frac{\partial}{\partial z}\right)\left(H_y - \frac{E_x}{\eta}\right) = 0, \tag{25}$$

$$L_{z+}^2 : \left(\frac{\partial}{\partial t} + c\frac{\partial}{\partial z}\right)\left(H_x - \frac{E_y}{\eta}\right) = 0, \tag{26}$$

$$L_{z-}^2 : \left(\frac{\partial}{\partial t} - c\frac{\partial}{\partial z}\right)\left(H_x + \frac{E_y}{\eta}\right) = 0, \tag{27}$$

where, $L_{m\pm}^s$ denotes the differential operators on m axis (m=x, y, z). Superscript s (=1,2) denotes an index of independent linear equations in each propagation direction and we will use this notation to describe the calculation procedure. The signs $\pm$ represent the forward or backward propagations of electromagnetic field in the associated m direction. Assuming that the medium is homogeneous and the propagation velocity c is constant at every points in analysis region, a set of differential equations in each direction can be found directly by differentiation with respect to x, y and z axes. The system of differential equations have the similar form with the above equations, e.g., the differentiation of (16) with respect to x axis gives,

$$\left(\frac{\partial}{\partial t} + c\frac{\partial}{\partial x}\right)\left(\partial_x H_z + \frac{\partial_x E_y}{\eta}\right) = 0. \tag{28}$$

Next we consider $H_z - E_y$ pairs of (16) and (17). Another pairs of the field components can be formulated in the same way. Figure 2 illustrates the concept of characteristic method for the field propagation. The field components H_z and E_y at the time step index n propagate forward or backward along the x axis, corresponding to the sign of velocity c. The forward propagating field components, which are calculated from the field values and its derivatives at grid points x_i and x_{i-1} by using the CIP method, are denoted by H_{z+}^n and E_{y+}^n, respectively. The backward propagating field components calculated by using the CIP method are denoted by H_{z-}^n and E_{y-}^n. After the field components propagating into the left and right region as shown in Fig. 2 are found, the

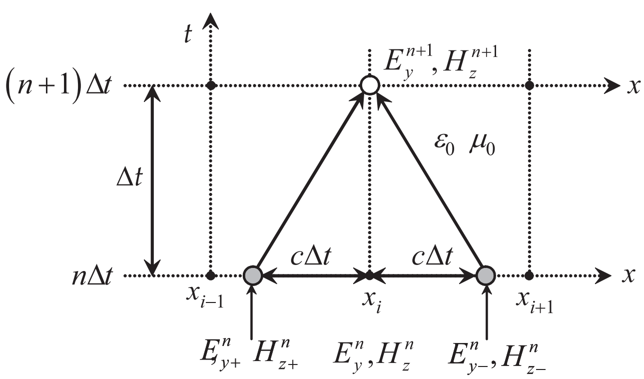

Fig. 2 Characteristic method for the calculation of the fields at the next time step.

fields at the grid point x_i are calculated by using the invariant of characteristic variables as

$$H_z^* + \frac{E_y^*}{\eta} = H_{z+}^n + \frac{E_{y+}^n}{\eta}, \tag{29}$$

$$H_z^* - \frac{E_y^*}{\eta} = H_{z-}^n - \frac{E_{y-}^n}{\eta}. \tag{30}$$

Solving (29) and (30) gives update equations for electric and magnetic fields at the grid point x_i in explicit forms as

$$E_y^* = \frac{1}{2}\left\{E_{y+}^n + E_{y-}^n + \eta H_{z+}^n - \eta H_{z-}^n\right\}, \tag{31}$$

$$H_z^* = \frac{1}{2}\left\{\frac{E_{y+}^n}{\eta} - \frac{E_{y-}^n}{\eta} + H_{z+}^n + H_{z-}^n\right\}, \tag{32}$$

where E_{y+}^n and H_{z+}^n are the field components located at $x_i + c\Delta t$ with the time step index, n, and propagating toward the grid point, x_i. Similarly, E_{y-}^n and H_{z-}^n are the field components located at $x_i - c\Delta t$ and propagating toward the same grid point, x_i. Superscript $*$ is used to represent the fields after propagating along the x axis as same as in Eq. (9). The equations in (31) and (32) are the update equations for the differential operator L_x^1. The update equations for the differential operator $L_x^2, L_y^1, L_y^2, L_z^1$, and L_z^2 can also be determined in the same way and can be expressed as follows. For L_x^2 operator,

$$E_z^* = \frac{1}{2}\left\{E_{z+}^n + E_{z-}^n - \eta H_{y+}^n + \eta H_{y-}^n\right\}, \tag{33}$$

$$H_y^* = \frac{1}{2}\left\{-\frac{E_{z+}^n}{\eta} + \frac{E_{z-}^n}{\eta} + H_{y+}^n + H_{y-}^n\right\}, \tag{34}$$

for L_y^1 operator,

$$E_x^{**} = \frac{1}{2}\left\{E_{x+}^* + E_{x-}^* - \eta H_{z+}^* + \eta H_{z-}^*\right\}, \tag{35}$$

$$H_z^{**} = \frac{1}{2}\left\{-\frac{E_{x+}^*}{\eta} + \frac{E_{x-}^*}{\eta} + H_{z+}^* + H_{z-}^*\right\}, \tag{36}$$

for L_y^2 operator,

$$E_z^{**} = \frac{1}{2}\left\{E_{z+}^* + E_{z-}^* + \eta H_{x+}^* - \eta H_{x-}^*\right\}, \tag{37}$$

$$H_x^{**} = \frac{1}{2}\left\{\frac{E_{z+}^*}{\eta} - \frac{E_{z-}^*}{\eta} + H_{x+}^* + H_{x-}^*\right\}, \tag{38}$$

for L_z^1 operator,

$$E_x^{n+1} = \frac{1}{2}\left\{E_{x+}^{**} + E_{x-}^{**} + \eta H_{y+}^{**} - \eta H_{y-}^{**}\right\}, \tag{39}$$

$$H_y^{n+1} = \frac{1}{2}\left\{\frac{E_{x+}^{**}}{\eta} - \frac{E_{x-}^{**}}{\eta} + H_{y+}^{**} + H_{y-}^{**}\right\}, \tag{40}$$

and for L_z^2 operator,

$$E_y^{n+1} = \frac{1}{2}\left\{E_{y+}^{**} + E_{y-}^{**} - \eta H_{x+}^{**} + \eta H_{x-}^{**}\right\}, \tag{41}$$

$$H_x^{n+1} = \frac{1}{2}\left\{-\frac{E_{y+}^{**}}{\eta} + \frac{E_{y-}^{**}}{\eta} + H_{x+}^{**} + H_{x-}^{**}\right\}, \tag{42}$$

where superscripts $**$ is used to describe the field components after propagating along the x and y axes. The update equations formulated above are equivalent to the determination of $\mathbf{W}$ by multiplying the similar matrix S_m with $S_m^{-1}\mathbf{W}$. It is interesting to note here that there is no field component aligned in the x, y, and z axes propagating along the same x, y, and z directions because they are corresponding to the associated eigenvalue of zero. The update equations formulated using the differential equations are determined in the same way, e.g., from (28) we obtain,

$$\partial_x E_y^* = \frac{1}{2}\left\{\partial_x E_{y+}^n + \partial_x E_{y-}^n + \eta\partial_x H_{z+}^n - \eta\partial_x H_{z-}^n\right\}, \tag{43}$$

$$\partial_x H_z^* = \frac{1}{2}\left\{\frac{\partial_x E_{y+}^n}{\eta} - \frac{\partial_x E_{y-}^n}{\eta} + \partial_x H_{z+}^n + \partial_x H_{z-}^n\right\}. \tag{44}$$

In addition to the formulation of the wave equations differentiated with respect to the x axis, the differentiations with respect to the axis perpendicular to the propagation direction, e.g., $\partial_z E_y$, and $\partial_z H_z$, must be also computed. Here we apply the first-order upwind scheme to those calculations as, for $c > 0$,

$$\partial_z E_{y+}^n(k) = \partial_z E_y^n(k) - \frac{c\Delta t}{\Delta y}\left(\partial_z E_y^n(k) - \partial_z E_y^n(k-1)\right), \tag{45}$$

$$\partial_z H_{z+}^n(k) = \partial_z H_z^n(k) - \frac{c\Delta t}{\Delta y}\left(\partial_z H_z^n(k) - \partial_z H_z^n(k-1)\right), \tag{46}$$

and for $c < 0$,

$$\partial_z E_{y+}^n(k) = \partial_z E_y^n(k) + \frac{c\Delta t}{\Delta y}\left(\partial_z E_y^n(k) - \partial_z E_y^n(k+1)\right), \tag{47}$$

$$\partial_z H_{z+}^n(k) = \partial_z H_z^n(k) + \frac{c\Delta t}{\Delta y}\left(\partial_z H_z^n(k) - \partial_z H_z^n(k+1)\right), \tag{48}$$

where Δt is the time step size, Δz is the cell size, and k is the grid index in z axis. Then, by using (45)–(48), $\partial_z E_y$ and $\partial_z H_z$ can be determined from equations with the same form as (43) and (44). $\partial_y E_y$ and $\partial_y H_z$ can be computed in the same manner. This kind of the CIP method is called "type-M CIP method" [13], which requires less memory compared to another type of the CIP method.

A cyclic sequence of one-dimensional operators is applied to maintain the symmetry of the solutions. The fields at the next time step $n+2$ can be then expressed by using the notation of the differential operators as,

$$\mathbf{W}^{n+1} = L_z^2 L_z^1 L_y^2 L_y^1 L_x^2 L_x^1 \mathbf{W}^n, \tag{49}$$
$$\mathbf{W}^{n+2} = L_x^1 L_x^2 L_y^1 L_y^2 L_z^1 L_z^2 \mathbf{W}^{n+1}. \tag{50}$$

The same sequence is also applied to the system equations of the differentiated field components.

3. Boundary Conditions in the CIP Method

In this section, boundary conditions for perfect conducting (PEC) interface and those between two media, and a boundary condition for suppression of reflected waves at truncated region are described.

3.1 Treatment of the Fields Close to the PEC Interface

Figure 3 shows an interface between free space and PEC object in one-dimensional domain. An incident plane wave is coming from right region with the velocity c. The PEC boundary is defined at a middle plane between two grid points, x_i and x_{i-1}. The electric field at the PEC boundary satisfies the condition:

$$\hat{\mathbf{n}} \times \mathbf{E} = 0, \tag{51}$$

where $\mathbf{E}$ is a total electric field and $\hat{\mathbf{n}}$ is a surface outward normal vector. The fields close to the interface can be determined by creating an image of the electromagnetic field at x_{i-1}, i.e.

$$\mathbf{E}_t^n(x_{i-1}) = -\mathbf{E}_t^n(x_i), \tag{52}$$
$$\mathbf{H}_t^n(x_{i-1}) = \mathbf{H}_t^n(x_i), \tag{53}$$

where, subscript t denotes the tangential field component. After the substitution of the field value at x_i is done, the CIP method is then applied to determine the field values at the next time step index, $n+1$, according to the update Eqs. (31)–(42).

3.2 Treatment of the Fields Close to the Interface between Two Different Media

Figure 4 shows the interface between two different media in one-dimensional domain. Only the formulation of $H_z - E_y$ pairs is described here and another pairs of the field components can be formulated in the same manner. The invariant of characteristic variables in two media is given by

$$H_z^* + \frac{E_y^*}{\eta_1} = H_{y+}^n + \frac{E_{y+}^n}{\eta_1}, \tag{54}$$
$$H_z^* - \frac{E_y^*}{\eta_2} = H_{y-}^n - \frac{E_{y-}^n}{\eta_2}. \tag{55}$$

By solving (54) and (55) for E_y^* and H_z^*, the update equations for electromagnetic fields at the dielectric interface are obtained and given by

$$E_y^* = \frac{\eta_1\eta_2}{\eta_1+\eta_2}\left\{\frac{E_{y+}^n}{\eta_1} + \frac{E_{y-}^n}{\eta_2} + H_{z+}^n - H_{z-}^n\right\}, \tag{56}$$
$$H_z^* = \frac{1}{\eta_1+\eta_2}\left\{E_{y+}^n - E_{y-}^n + \eta_1 H_{z+}^n + \eta_2 H_{z-}^n\right\}, \tag{57}$$

where η_1, η_2 are the intrinsic impedances in media #1 and #2, respectively. It should be noted that the update equations for the differential field values have the similar form as (56) and (57).

3.3 Boundary Conditions at Truncated Region

Since the CIP method calculates the field translation in each propagation direction individually, the reflection at the truncated region can be suppressed using the information of the propagation direction. Only incoming waves from the far field are set to be the null value at the truncated region as

$$\mathbf{W}_{x+}^n(0,j,k) = \mathbf{W}_{x-}^n(\mathrm{NX}-1,j,k) = 0, \tag{58}$$
$$\mathbf{W}_{y+}^n(i,0,k) = \mathbf{W}_{y-}^n(i,\mathrm{NY}-1,k) = 0, \tag{59}$$
$$\mathbf{W}_{z+}^n(i,j,0) = \mathbf{W}_{z-}^n(i,j,\mathrm{NZ}-1) = 0, \tag{60}$$

where $\mathbf{W}_{m+}^n(i,j,k)$ and $\mathbf{W}_{m-}^n(i,j,k)$ are the field component

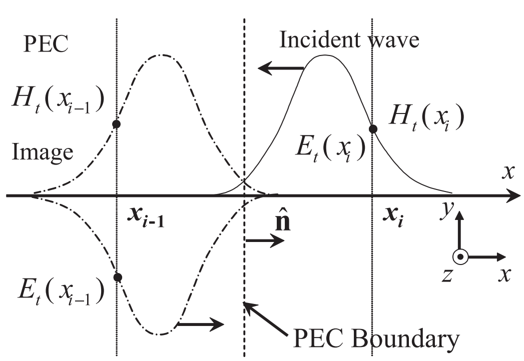

Fig. 3 Boundary condition for PEC object.

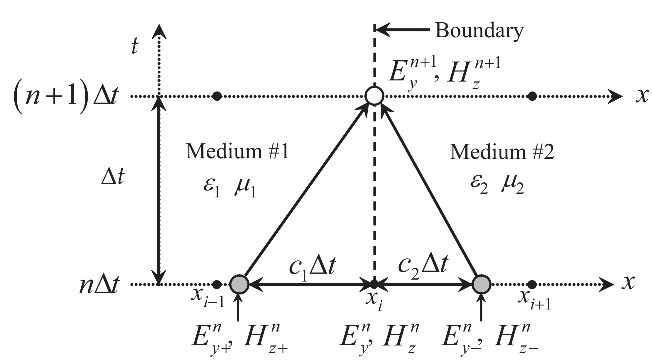

Fig. 4 Boundary condition between two different dielectric medium.

vectors at the grid location index, (i, j, k), and the time step index, n, which are propagating forward and backward, respectively, along the m ($m = x,y,z$) axis from the far region into the analysis region. NX, NY, and NZ are total numbers of the discretization of the analysis region in the x, y, and z axes, respectively. This boundary condition is well-posed only when the propagation direction of electromagnetic wave is aligned with Cartesian coordinate system. When the propagation direction is not aligned with Cartesian coordinate system, the exact no-reflection boundary condition is degraded to an approximation and it behaves like the first-order Mur's absorbing boundary condition (ABC). This is because only the electromagnetic waves propagating along the direction normal to the truncated boundary surface are transmitted without reflections as same as the first-order Mur's ABC [14].

4. Numerical Results

In order to confirm the validity of the proposed algorithms, the bistatic scattering cross sections (BSCS) of PEC sphere, dielectric sphere, and PEC cube are calculated using the CIP method and compared with the results calculated by the Mie's series and the FDTD method.

Figure 5 shows analysis models of PEC sphere and dielectric sphere for the CIP method. The radius of the spheres is $a = 5$ cm, the size of analysis region is 30 cm × 30 cm × 30 cm, and the cell sizes are 1 mm × 1 mm × 1 mm in x, y, and z directions, respectively. The incident plane wave is assumed to be a rectangular pulse wave with a pulse width of 5Δ, where Δ denotes the cell size in each axis. The information of the propagation is incorporated to suppress the reflected field at the outermost boundary as describe in Sect. 3.3. The reason for using the rectangular pulse as an incident plane wave in the CIP method is that because the interpolation using third-order polynomials is applied in the CIP method, so that the CIP method can represent the rectangular waveform more accurately than the Gaussian waveform which is actually used in the FDTD method. The CIP method can treat the waveform which changes abruptly with respect to time. This is also one of the advantages of the CIP method.

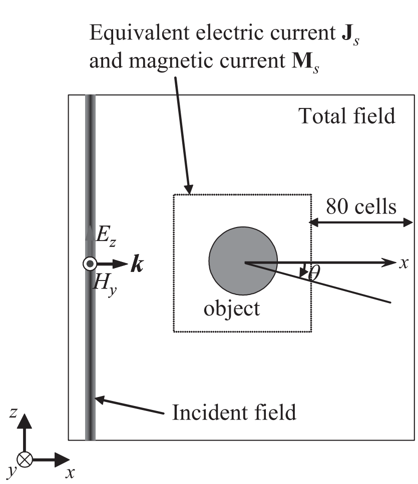

Fig. 5 Analysis model for CIP method.

Figure 6 shows the analysis model used for the FDTD analysis. The radius of the spheres, the size of analysis region and the cell sizes are the same to those in the CIP model. Total-field/scattered-field (TF/SF) boundary [2] is applied to illuminate the plane wave into the analysis region. A perfectly matched layer (PML) is also used to suppress the reflection of electromagnetic waves at the outermost boundary. Gaussian waveform with a pulse width of $\tau_0 = 133$ nsec. and an attenuation constant of $\alpha = 16/\tau_0^2$ is employed as an incident plane wave.

The Courant-Friedrich-Levy (CFL) number is defined as $\mathrm{CFL} = c\Delta t/\Delta$ for the CIP method, where Δt is the time step size. Since the maximum time step size is restricted by the Courant stability condition [2], so that the maximum CFL number for the FDTD model is about $1/\sqrt{3}= 0.577$ but it is unity for the CIP model, which means that the CIP method requires less time steps compared with the FDTD method. Parameters for the numerical analyses are summarized in Table 1.

In order to calculate the BSCS evaluated by the far-zone field, the equivalent electric surface currents, $\mathbf{J}_s$, and magnetic surface currents, $\mathbf{M}_s$, located on a cubic surface encompassing the sphere are used as shown in Figs. 5 and 6. Since the outermost boundary of the CIP model behaves like the first-order Mur's ABC in the FDTD method, the re-

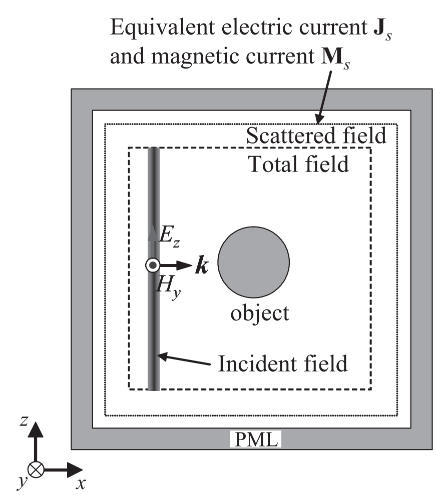

Fig. 6 Analysis model for FDTD method.

Table 1 Parameters for analysis.

	CIP method	FDTD method
Analysis region	300×300×300 cells	300×300×300 cells
Cell size $\Delta x,\Delta y,\Delta z$	1 mm	1 mm
Analysis frequency	5 GHz, 10 GHz	5 GHz, 10 GHz
CFL number	1	0.5762
Incident pulse	rectangular pulse	gaussian pulse
ABC	None	8-layer PML
Number of time steps	500 (PEC case)	1500 (PEC case)

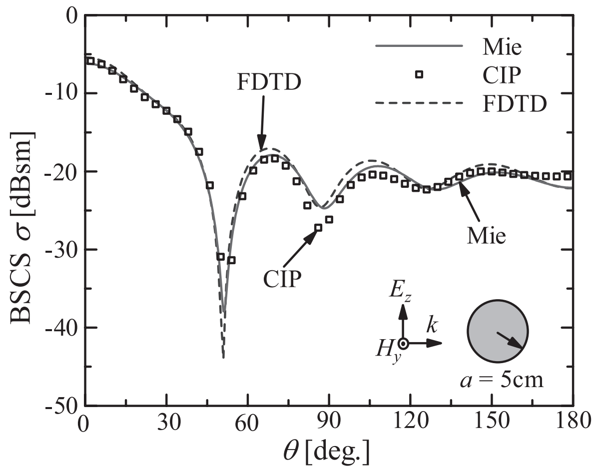

Fig. 7 BSCS of PEC sphere with radius of 5 cm at 5 GHz.

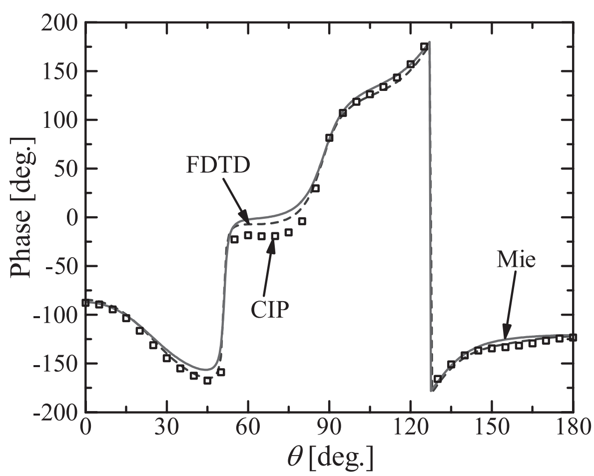

Fig. 8 Phase of μ_s of PEC sphere with radius of 5 cm at 5 GHz.

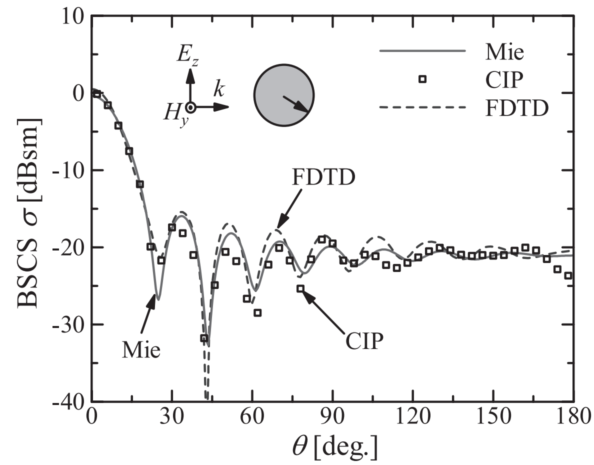

Fig. 9 BSCS of PEC sphere with radius of 5 cm at 10 GHz.

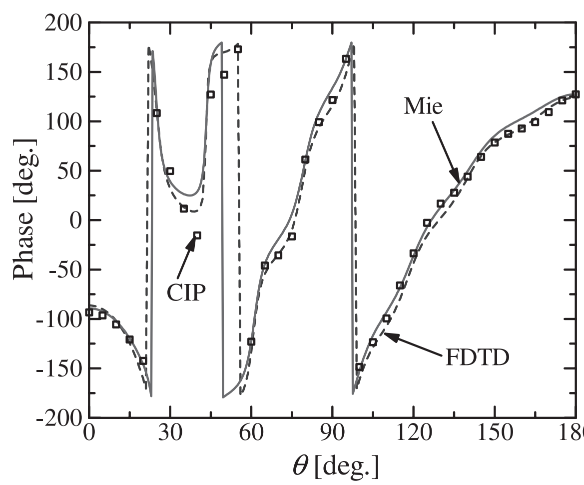

Fig. 10 Phase of μ_s of PEC sphere with radius of 5 cm at 10 GHz.

flected wave will appear and degrade accuracy of the analysis when the incident angle of electromagnetic fields is not normal to the boundary. To avoid this problem, the equivalent current surfaces are placed far enough from the outermost boundary, i.e. 80 cells from the outermost boundary in our simulation. Finally, the bistatic scattering coefficient is calculated by the following equation.

$$\mu_s = \lim_{r\to\infty} 2\sqrt{\pi} r \frac{E^s}{E^{\text{inc}}}, \tag{61}$$

where, E^{inc} represents the incident electric field and E^s represent the scattered electric field.

Figures 7 and 8 show the BSCS $\sigma = |\mu_s|^2$ and the phase of the scattering coefficient of the PEC sphere at 5 GHz by using the CIP and the FDTD methods. The analysis results at 10 GHz are also shown in Figs. 9 and 10. The results at both 5 and 10 GHz are obtained simultaneously via discrete Fourier transform of the electric and magnetic fields on the closed surface. The scattering coefficient at another frequencies can also be calculated easily by one single-pulse excitation, which is one of the advantages of the time-domain method. The exact solutions for the BSCS and the phase of the scattering coefficient obtained by the Mie's series are also plotted by the solid line in these figures. The FDTD results are plotted by the dashed line. The results obtained by both the CIP and the FDTD methods show good agreements with the Mie's results for PEC sphere case. However, the reflected waves from the outermost boundary are still observed and affect the bistatic scattering coefficient amplitude as $\theta = 30° - 60°$ in the CIP model.

As a second example of the scattering analysis using the CIP method, the scattering coefficient of the dielectric sphere with the radius of $a = 5$ cm is calculated. Figures 11 and 12 show the BSCS and the phase of the scattering coefficient of the dielectric sphere at 5 GHz and Figs. 13 and 14 show those at 10 GHz. The results calculated by the FDTD method and the exact solution by the Mie's series are also plotted in the figures. It is seen that the results computed by the CIP method for the dielectric sphere are more accurate than those for the PEC sphere because the reflected waves from the outermost boundary of the CIP model are less than that in the case of the PEC sphere. It should be also no-

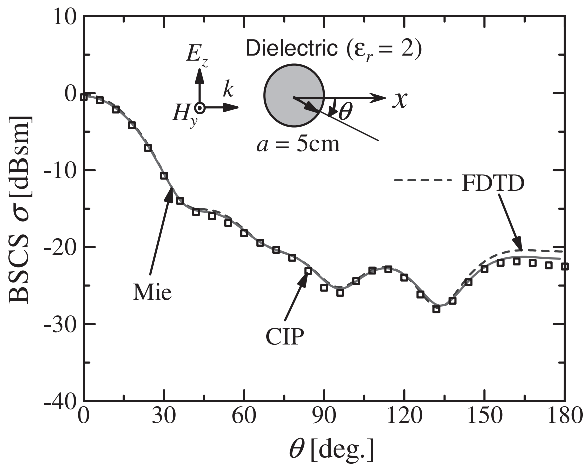

Fig. 11 BSCS of dielectric sphere with radius of 5 cm at 5 GHz.

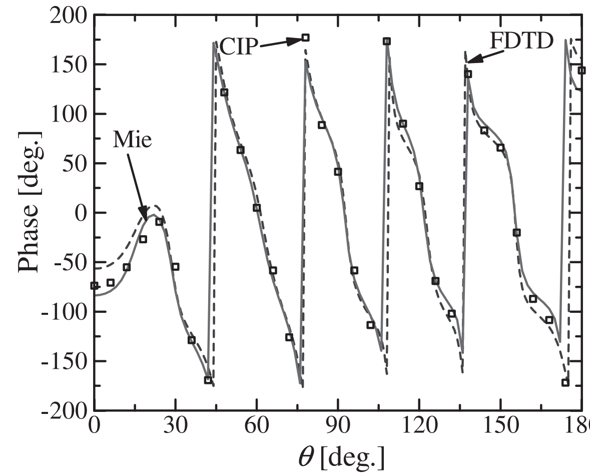

Fig. 14 Phase of μ_s of dielectric sphere with radius of 5 cm at 10 GHz.

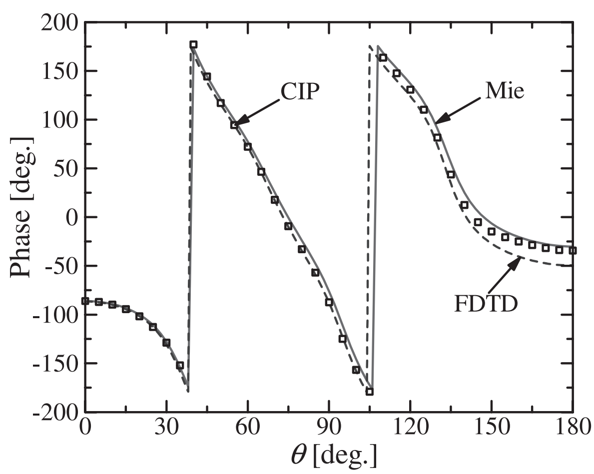

Fig. 12 Phase of μ_s of dielectric sphere with radius of 5 cm at 5 GHz.

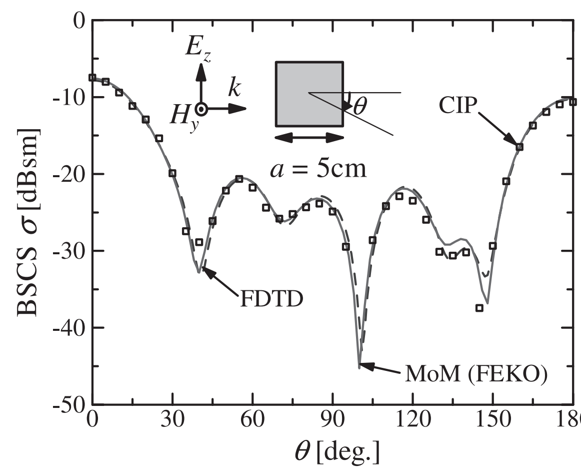

Fig. 15 BSCS of a cube with side length of 5 cm at 10 GHz.

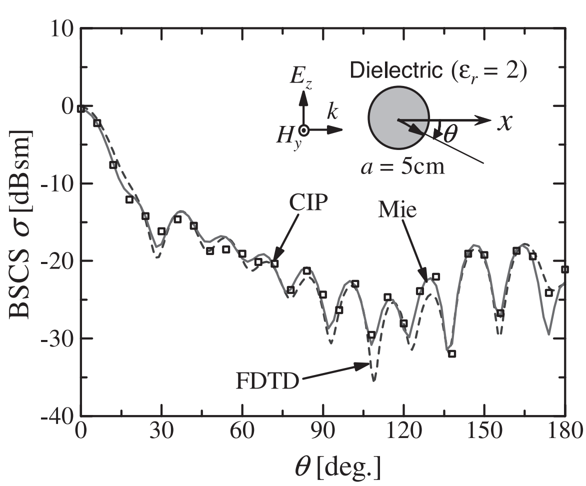

Fig. 13 BSCS of dielectric sphere with radius of 5 cm at 10 GHz.

ticed that the phase of scattering coefficient obtained by the CIP method is slightly more accurate than that of the FDTD method for θ close to $0°, 180°$. This is due to the fact that the FDTD method suffers from the phase error caused by the anisotropy especially at $\theta = 0°$ and $180°$, where the electromagnetic wave penetrates into dielectric material. Although the decrease in the accuracy of the FDTD analysis is not so important in the present model, it could be more serious when the analysis domain is very large and the information of propagation phase is very important. This observation shows that the CIP method could be an alternative method for a large analysis model.

As a third example, the CIP method was applied to the numerical analysis of the electromagnetic scattering of a PEC cube with one-side length of 5 cm. The model for the analysis is the same to Figs. 5 and 6 except that the sphere is replaced with the cube. Since the exact solution is not available for the PEC cube case, the method of moment (MoM) and the FDTD method was employed and their results are compared with the CIP results. The MoM analysis was performed by a commercial electromagnetic analysis simulation software called FEKO. The BSCS and the phase of scattering coefficient for the PEC cube are shown in Figs. 15 and 16. It can be seen that the CIP results agree well with

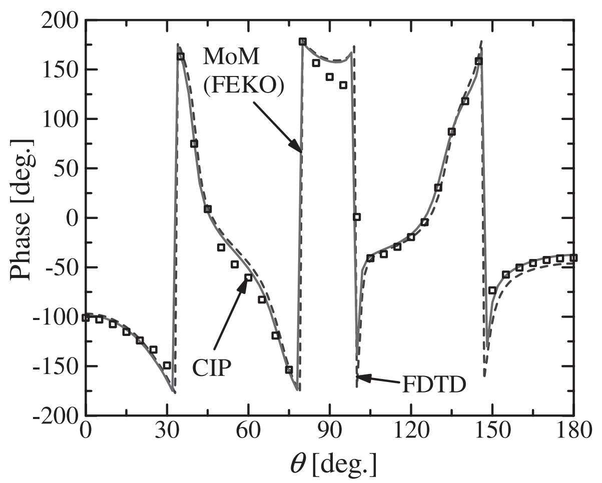

Fig. 16 Phase of μ_s of cube with side length of 5 cm at 10 GHz.

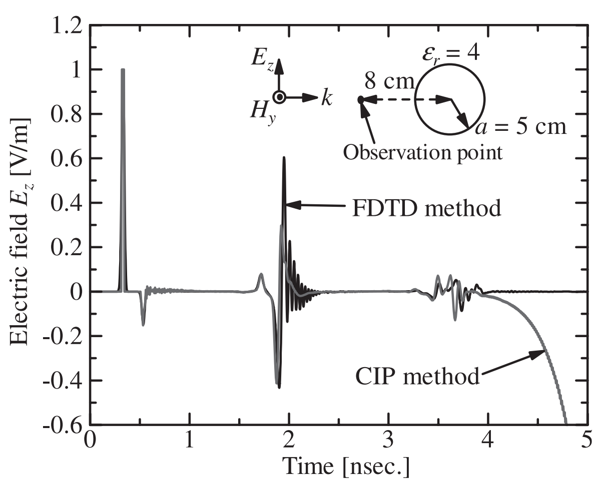

Fig. 17 Instability in the CIP method.

those obtained by the FDTD method and the MoM, which again confirms the validity of CIP method.

Although the CIP method can be used to calculate the SCS of the dielectric sphere with a small permittivity as demonstrated above, the CIP method becomes unstable when dielectric constant becomes higher. As an example, Fig. 17 shows the electric field strength E_z with respect to the time for the CIP and FDTD method for the case of the dielectric sphere with $\varepsilon_r = 4$.

The reason for the instability is that the update equations expressed in (56) and (57) for the interface between two dielectrics is an approximation for the case that spatial changes of the permittivity are small. For example, the differentiation of (16) and (17) gives following equations: for L^1_{x+} operator,

$$\left(\frac{\partial}{\partial t} + c\frac{\partial}{\partial x}\right)\left(\partial_x H_z + \frac{\partial_x E_y}{\eta_1}\right) = -\frac{\partial c}{\partial x}\left(H_z + \frac{\partial E_y}{\eta_1}\right), \quad (62)$$

and for L^1_{x-} operator,

Table 2 Number of time steps before divergence.

	Number of time steps before divergence			
	$\varepsilon_r = 2$	$\varepsilon_r = 4$	$\varepsilon_r = 6$	$\varepsilon_r = 10$
Δx=Δy=Δz=1 mm	> 1300	1160	950	640

Table 3 CPU time and memory usage for the CIP and FDTD methods.

	CPU time [sec.]		Memory usage [Mbytes]	
Number of cells	CIP	FDTD	CIP	FDTD
200×200×200	2178	507	1760	940.5
(per step)	2.185	0.29		
300×300×300	3310	1216	5940	2732
(per step)	3.303	0.695		

$$\left(\frac{\partial}{\partial t} - c\frac{\partial}{\partial x}\right)\left(\partial_x H_z - \frac{\partial_x E_y}{\eta_2}\right) = \frac{\partial c}{\partial x}\left(H_z - \frac{\partial E_y}{\eta_2}\right). \quad (63)$$

In our formulations, the spatial derivative of the propagation velocity or $\frac{\partial c}{\partial x}$ is considered to be small enough to be neglected so that the right-hand term is equal to zero. However, for a high-permittivity dielectric case, this term can not be neglected and it causes the instability in our simulation.

Next, the effect of the permittivity value and the cell size to the stability of the CIP method is demonstrated. Number of the time steps which the solutions are stable for each value of the permittivity is determined from the time-domain plot and the results are summarized in Table 2. From the Table 2, it is seen that when the permittivity of the sphere become higher, the CIP method becomes more unstable. Although the instability can be relieved by using a larger cell size, the changing in the cell size also affect accuracy of discretization of the model so that it is impractical in some case. Improvement of the stability of the CIP method at the interface between dielectrics is also a part of our future works.

Finally, calculation time and memory usage for the CIP and FDTD methods are shown in Table 3. All programs are run on the SX-9 supercomputer in Tohoku University, Japan. From the Table, it is seen that CPU time for the CIP method is longer than that for the FDTD method since the calculation using the CIP method is the two-step scheme as described above. Although the CIP method requires fewer time step, the computations at each step are more expensive than the FDTD method. Moreover the memory usage for the CIP method is about 2 times of the FDTD method because the CIP method needs to store both the field values and the differential field values. The memory usage for the CIP method can be approximately determined from the following equation;

$$\begin{aligned}\text{Memory usage} = \; & 24 \times \mathrm{NX} \times \mathrm{NY} \times \mathrm{NZ} \times 8 \\ & +3 \times \mathrm{NX} \times \mathrm{NY} \times \mathrm{NZ} \times 8 \\ & +4 \times \mathrm{NX} \times \mathrm{NY} \times \mathrm{NZ}\end{aligned}$$

The first term is for the variables of the field components and their differential field components. The second term is for the constants at each grid points (intrinsic impedance, propagation velocity, permittivity of medium). The last term is for material index at each grid points.

5. Conclusion

The characteristic-based CIP method for solving three-dimensional Maxwell's equations has been developed. The boundary conditions for PEC and dielectric interfaces have been formulated and implemented successfully. The CIP method is then applied to the analysis of the scattering from the PEC sphere and the dielectric sphere and compared with the exact solutions and the FDTD results. It is also applied to the scattering from the PEC cube and compared with the FDTD and the MoM results. The agreement of the present results is fairly good with the exact analytic results, which demonstrates the validity of the CIP method. Although a stability problem is still remained, it has been shown that CIP method can be an alternative numerical technique for solving electromagnetic problems and could broaden the field of the CEM.

Extension of Cartesian grid-based system to the body-fitted coordinate system with the utilization of Jacobian coordinate transformation is remaining work to increase the accuracy.

Acknowledgement

This work was partly supported by Tohoku University 21st Century Center of Excellent (COE) program. Parts of the numerical results in this research were obtained by using supercomputing resources at Information Synergy Center, Tohoku University.

References

[1] K.S. Yee, "Numerical solution of initial boundary value problems involving Maxwell's equations in isotropic media," IEEE Trans. Antennas Propag., vol.AP-14, no.4, pp.302–307, 1966.
[2] A. Taflove, Computational Electrodynamics, The Finite-Difference Time-Domain Method, Artech House Publisher, 1995.
[3] J.S. Shang, "A fractional-step method for solving 3D, time-domain Maxwell equations," J. Comput. Phys., vol.118, pp.109–119, 1995.
[4] J.S. Shang, "Characteristic-based algorithms for solving the Maxwell equations in the time domain," IEEE Antennas Propag. Mag., vol.37, no.3, pp.15–25, June 1995.
[5] J.S. Shang and R.M. Fithen, "A comparative study of characteristic-based algorithms for the Maxwell equations," J. Comput. Phys., vol.125, pp.378–394, 1996.
[6] J.S. Shang and D. Gaitonde, "Characteristic-based, time-dependent Maxwell equations solvers on a general curvilinear frame," AIAA J., vol.33, no.3, pp.491–498, 1995.
[7] J.S. Shang, "Shared knowledge in computational fluid dynamics, electromagnetics, and magneto-aerodynamics," Progress in Aerospace Sciences, vol.38, pp.449–467, 2002.
[8] D. Jiao, J.-M. Jin, and J.S. Shang, "Characteristic-based finite-volume time-domain method for scattering by coated objects," Electromagnetics, vol.20, pp.257–268, 2000.
[9] H. Takewaki, A. Nishigushi, and T. Yabe, "Cubic interpolated pseudo-particle method (CIP) for solving hyperbolic-type equations," J. Comput. Phys., vol.61, no.2, pp.261–268, Nov. 1985.
[10] Y. Ogata, T. Yabe, and K. Odagaki, "An accurate numerical scheme for Maxwell equation with CIP-method of characteristics," Comm. Comput. Phys., vol.1, no.2, pp.311–335, April 2006.
[11] T. Utsumi, T. Kunugi, and T. Aoki, "Stability and accuracy of the cubic interpolated propagation scheme," Comput. Phys. Commun., vol.101, pp.9–20, 1997.
[12] K. Okubo and N. Takeuchi, "Analysis of an electromagnetic field created by line current using constrained interpolation profile method," IEEE Trans. Antennas Propag., vol.55, no.1, pp.111–119, Jan. 2007.
[13] T. Yabe, T. Utsumi, and Y. Ogata, The Constrained Interpolation Profile Method, Morikita Publishing, Tokyo, Japan, 2003.
[14] G. Mur, "Absorbing boundary conditions for the finite-difference approximation of the time domain electromagnetic field equations," IEEE Trans. Electromagn. Compat., vol.EMC-31, no.139, pp.629–651, Nov. 1981.
[15] R.F. Harrington, Time-Harmonic Electromagnetic Field, The IEEE Press Series on Electromagnetic Wave Theory, Wiley-Interscience, 2001.

Jerdvisanop Chakarothai received the B.E. degree from Akita University, Akita, Japan, in 2003, the M.E. degrees from Tohoku University, Sendai, Japan, in 2005. He is currently pursuing the Ph.D. degree in electrical and communication engineering at Tohoku University. His research interests include computational electromagnetics (CEM), electromagnetic compatibility, EM inverse problems and antenna measurement. He is a member of the IEEE.

Qiang Chen received the B.E. degree from Xidian University, Xi'an, China, in 1986, the M.E. and D.E. degrees from Tohoku University, Sendai, Japan, in 1991 and 1994, respectively. He is currently and Associate Professor with the Department of Electrical Communications, Tohoku University. His primary research interests include computational electromagnetics, adaptive array antennas, and antenna measurement. Dr. Chen received the Young Scientists Award in 1993 from the Institute of Electronics, Information and Communication Engineers (IEICE) of Japan. He has served as the Secretary and Treasurer of IEEE AP-S Japan Chapter in 1998, the Secretary of Technical Committee on Electromagnetic Compatibility of IEICE from 2004 to 2006. Dr. Chen is a member of the IEEE, and the Institute of Image Information and Television Engineers of Japan.

Kunio Sawaya received the B.E., M.E., and D.E. degrees from Tohoku University, Sendai, Japan, in 1971, 1973 and 1976, respectively. He is presently a Professor in the Department of Electrical and Communication Engineering at the Tohoku University. His areas of interests are antennas in plasma, antennas for mobile communications, theory of scattering and diffraction, antennas for plasma heating, and array antennas. He received the Young Scientists Award in 1981 and the Paper Awards in 1988 and 2006 both from the Institute of Electronics, Information and Communcation Engineers (IEICE) of Japan. He served as the Chairperson of the Technical Group of Antennas and Propagation of the IEICE from 2001 to 2003 and the Chairperson of the Organizing and Steering Committees of 2004 International Symposium on Antennas and Propagation (ISAP'04). Dr. Sawaya is a senior member of the IEEE, and a member of the Institute of Image Information and Television Engineers of Japan.